

Geochemistry, Geophysics, Geosystems[®]



RESEARCH ARTICLE

10.1029/2024GC011508

Key Points:

- Sr/Ca ratios in *P. wuellerstorfi* show no detectable influence of temperature and are useful for reconstructing changes in ΔCO_3
- S/Ca ratios in *P. wuellerstorfi* may potentially be used to reconstruct a long-term (e.g., Cenozoic) record of sulfate in the ocean
- Sr/Ca derived ΔCO_3 records suggest CO_2 release from upper water and then from progressively deeper water during the last three terminations

Supporting Information:

Supporting Information may be found in the online version of this article.

Correspondence to:

V. J. Lawson,
vera.lawson@rutgers.edu



Citation:

Lawson, V. J., Rosenthal, Y., Bova, S. C., Lambert, J., Linsley, B. K., Bu, K., et al. (2024). Controls on Sr/Ca, S/Ca, and Mg/Ca in benthic foraminifera: Implications for the carbonate chemistry of the Pacific Ocean over the last 350 ky. *Geochemistry, Geophysics, Geosystems*, 25, e2024GC011508. <https://doi.org/10.1029/2024GC011508>

Received 12 FEB 2024

Accepted 23 JUL 2024

Controls on Sr/Ca, S/Ca, and Mg/Ca in Benthic Foraminifera: Implications for the Carbonate Chemistry of the Pacific Ocean Over the Last 350 ky

V. J. Lawson^{1,2} , Y. Rosenthal^{1,2} , S. C. Bova³ , J. Lambert^{4,5}, B. K. Linsley⁴ , K. Bu², V. J. Clementi² , A. Elmore⁶ , and E. L. McClymont⁷ 

¹Department of Earth and Planetary Sciences, Rutgers, The State University of New Jersey, Piscataway, NJ, USA,

²Department of Marine and Coastal Sciences, Rutgers, The State University of New Jersey, New Brunswick, NJ, USA,

³Department of Earth and Environmental Sciences, San Diego State University, San Diego, CA, USA, ⁴Lamont-Doherty Earth Observatory, Columbia University, Palisades, NY, USA, ⁵Department of Earth and Environmental Sciences, Columbia University, New York, NY, USA, ⁶National Oceanic and Atmospheric Administration Ocean Exploration, Silver Spring, MD, USA, ⁷Department of Geography, Durham University, Durham, England

Abstract Boron to calcium (B/Ca) records in benthic foraminifera, used for reconstructing the carbonate ion saturation state (ΔCO_3) of the deep ocean, suggest that carbon sequestration in the Southern Pacific contributed to lowering atmospheric CO_2 during the last glacial interval. However, the spatial and temporal extent of this storage is debated due to limited ΔCO_3 records. To increase available ΔCO_3 records, we explored using strontium and sulfur to calcium (Sr/Ca, S/Ca) in *Planulina wuellerstorfi* as additional proxies for ΔCO_3 based on comparison with paired B/Ca down-core records from Pacific Sites U1486 (1,332 m depth) and U1487 (874 m depth) cored during the International Ocean Discovery Program Expedition 363. The Sr/Ca and S/Ca records from *P. wuellerstorfi* closely covary with the B/Ca-derived ΔCO_3 records. Temperature, reconstructed using *Uvigerina peregrina* magnesium to calcium (Mg/Ca), has no discernible effect on Sr/Ca, whereas S/Ca also varies with Mg/Ca in both *U. peregrina* and *P. wuellerstorfi*, suggesting an additional temperature effect. Mg/Ca records from *P. wuellerstorfi* are affected by both temperature and ΔCO_3 . We assess calibrations of Sr/Ca to ΔCO_3 for the Atlantic, Pacific, and Indian Oceans and recommend using the down-core rather than core-top calibrations as they yield consistent sensitivity, though with offsets, in all ocean basins. Reconstructing Pacific ΔCO_3 records from sites U1486, U1487, and DSDP 593, we demonstrate the benefit of using Sr/Ca as an additional ΔCO_3 proxy to assess the contribution of the Southern Pacific to the increase of atmospheric CO_2 at glacial terminations.

Plain Language Summary Burning of fossil fuels has increased since the industrial revolution, resulting in the addition of CO_2 , a gas which retains heat, to the atmosphere. Understanding how the earth's oceans work to regulate levels of atmospheric CO_2 is key to understanding the effects of increased atmospheric CO_2 on the earth's climate. The carbonate system in the ocean, of which CO_2 is a component, is complex. Carbonate saturation state (ΔCO_3) is a measure of how close the carbonate ion concentration is to the level at which calcite (which makes up the shell or test of some single-cell organisms) will dissolve. It is related to the level of ocean storage of CO_2 . Boron to calcium ratios (B/Ca) found in test calcite have been used as a proxy for past ocean ΔCO_3 , but these records are limited. Here, to increase presently available ΔCO_3 proxy records, we explore using strontium and sulfur to calcium (Sr/Ca, S/Ca) as additional proxies for ΔCO_3 . Unlike S/Ca, Sr/Ca shows no temperature influence, so makes a useable proxy for change in ΔCO_3 . Sr/Ca records can be used to infer the progressive release of oceanic CO_2 to the atmospheric at three terminations, periods in the past when atmospheric CO_2 increased dramatically.

1. Introduction

As the ocean is the largest carbon reservoir that can explain glacial-interglacial changes in atmospheric carbon dioxide, reconstruction of carbonate saturation in seawater is critical for understanding past changes in the carbon cycle. Such reconstructions have become available because carbonate saturation may influence the incorporation of trace elements into foraminiferal test calcite (Elderfield et al., 2006; Rosenthal et al., 2006; van Dijk et al., 2017; Yu & Elderfield, 2007; Yu, Elderfield, et al., 2014). Specifically, previous studies have shown that the incorporation of trace elements into foraminiferal tests is not strictly controlled by thermodynamic effects but is

© 2024 The Author(s). Geochemistry, Geophysics, Geosystems published by Wiley Periodicals LLC on behalf of American Geophysical Union. This is an open access article under the terms of the [Creative Commons Attribution License](https://creativecommons.org/licenses/by/4.0/), which permits use, distribution and reproduction in any medium, provided the original work is properly cited.

also influenced by biological or kinetic effects (Erez, 2003; Rosenthal et al., 1997). Because the exact mechanisms are presently not fully understood, empirical calibrations have been used to establish the use of trace elements in benthic foraminifera as proxies for seawater properties, such as magnesium/calcium (Mg/Ca) and boron/calcium (B/Ca) for temperature and carbonate saturation state, respectively (e.g., Lear et al., 2002; Nürnberg et al., 1996; Rosenthal et al., 1997; Yu & Elderfield, 2007). Since culturing experiments of deep-sea benthic foraminifera conducted in pressurized chambers are novel (Wollenburg et al., 2015), the calibrations rely on either core-top or down-core records. These have shown that the effects of temperature and saturation (where saturation is expressed as $\Delta\text{CO}_3 = [\text{CO}_3^{2-}]_{\text{observed}} - [\text{CO}_3^{2-}]_{\text{saturated}}$) on distribution coefficients are intertwined for benthic foraminifera found in cold deep waters with minimally saturated to unsaturated carbonate ion conditions (Elderfield et al., 2006; Rosenthal et al., 2006; Yu & Elderfield, 2008).

To date, B/Ca has been established as a carbonate saturation proxy for ΔCO_3 , calibrated empirically for *Planulina wuellerstorfi* using global core-top data (Yu & Elderfield, 2007), and used to reconstruct glacial-interglacial variations in deep ocean carbonate chemistry with implications for atmospheric CO_2 (Allen et al., 2020; Yu et al., 2010; Yu, Anderson, & Rohling, 2014; among others). Inorganic precipitation experiments suggest that (a) borate, $\text{B}(\text{OH})_4^-$, substitutes for carbonate, CO_3^{2-} , in calcite; (b) the partition coefficient depends on bicarbonate concentration, $[\text{HCO}_3^-]$; and (c) calcite B/Ca is influenced by seawater $[\text{B}(\text{OH})_4^-]/[\text{HCO}_3^-]$ (Hemming & Hanson, 1992). However, B/Ca measurements from core-top *P. wuellerstorfi* calcite do not show a pattern similar to seawater $[\text{B}(\text{OH})_4^-]/[\text{HCO}_3^-]$ (Yu & Elderfield, 2007). Though controls on the partitioning of boron into foraminiferal calcite are uncertain (Allen et al., 2012; Uchikawa et al., 2015), and calcification is probably not taking place directly from seawater but from an internal pool under biological control (Erez, 2003), there is strong empirical evidence of B/Ca dependence on seawater ΔCO_3 (Yu & Elderfield, 2007).

Postulated control of seawater ΔCO_3 on strontium/calcium (Sr/Ca) in foraminiferal calcite has led to the suggestion that Sr/Ca records, which are more readily available than B/Ca, may be used as an auxiliary carbonate system proxy (Keul et al., 2017; Yu, Elderfield, et al., 2014). The mechanism behind this effect is not clear, and unlike boron, Sr^{2+} is substituting for Ca^{2+} in the calcite lattice with no obvious dependence on CO_3^{2-} . Moreover, calibrations using paired core-top Sr/Ca and B/Ca from *P. wuellerstorfi* are offset between the Atlantic and Pacific Oceans, raising the possibility of secondary effects (Lo Giudice Cappelli et al., 2015; Yu, Elderfield, et al., 2014). Yu and Elderfield et al. (2014) found no correlation between temperature and Sr/Ca in core-top foraminiferal calcite. Studying Indo-Pacific core tops, Lo Giudice Cappelli et al. (2015) reported that temperature exhibits negligible control on Sr/Ca when temperatures are above 3°C, and that below 3°C, the higher sensitivity of Sr/Ca to temperature reflects a carbonate ion effect. For now, the temperature effect on Sr/Ca in benthic foraminiferal test calcite remains unclear.

It has also been argued that foraminiferal sulfur/calcium (S/Ca) reflects changes in the carbonate system (van Dijk et al., 2017), although a temperature effect on S/Ca cannot be ruled out (Berry, 1998). Like borate, sulfate, SO_4^{2-} , may substitute for CO_3^{2-} in test calcite (Pingitore et al., 1995). If SO_4^{2-} from seawater is the immediate source of the S/Ca found in foraminiferal calcite, S/Ca would have a distribution coefficient proportional to seawater $[\text{SO}_4^{2-}]/[\text{CO}_3^{2-}]$, decreasing as $[\text{CO}_3^{2-}]$ increases if $[\text{SO}_4^{2-}]$ in seawater remains constant. In a culturing study using shallow benthic foraminifera, S/Ca correlated negatively with $[\text{CO}_3^{2-}]$, consistent with the substitution of a lattice carbonate ion with a sulfate ion directly from seawater (van Dijk et al., 2017). However, in benthic foraminiferal calcite living deeper than 600 m, the S/Ca positively correlates with seawater temperature or $[\text{CO}_3^{2-}]$ (Berry, 1998), demonstrating that the biomineralization process that incorporates sulfur into benthic test calcite is not well understood, and suggesting that deep benthic foraminifera may control the calcification process differently than shallow benthic or planktic foraminifera.

Mg/Ca from the infaunal *Uvigerina* spp. is thought to reliably record the bottom temperature with no significant carbon saturation state effects (Elderfield et al., 2006, 2010; McClymont et al., 2016; Stirpe et al., 2021). In contrast, Mg/Ca ratios in *P. wuellerstorfi*, which show temperature effects (Lear et al., 2002) and have been used as a proxy for deep ocean temperature in the Atlantic (Ford et al., 2016; Martin et al., 2002; Sosdian & Rosenthal, 2009), also show carbonate saturation effects under low saturation state conditions. The effect of the carbon saturation state on epifaunal *P. wuellerstorfi* Mg/Ca in the Pacific and Indian oceans where the saturation state conditions are low, however, remains unclear (Lo Giudice Cappelli et al., 2015).

Here, we reconstruct the western equatorial Pacific intermediate and upper deep water carbonate saturation state from *P. wuellerstorfi* B/Ca records, and bottom water temperature (BWT) from *Uvigerina peregrina* Mg/Ca records spanning the last three glacial to interglacial (G-IG) cycles (350–0 ky). Then, we used these records to test the intertwined effects of carbonate saturation state and temperature on Sr/Ca, S/Ca, and Mg/Ca in *P. wuellerstorfi* calcite obtained from the same down-core samples. The down-core covariance among all the trace element records is used to determine the sensitivity of Sr/Ca and S/Ca to both ΔCO_2 and temperature. We further add core-top and additional down-core Sr/Ca data to generate specific calibrations to ΔCO_2 and demonstrate the advantage of using multiple ΔCO_2 proxies in understanding the contributions of the Southern Pacific Ocean to G-IG variations in atmospheric CO_2 over the past 350 ky.

2. Materials and Methods

2.1. Oceanographic Setting

International Ocean Discovery Program Expedition 363 Sites U1486 and U1487 are located in the western Bismarck Sea north of Papua New Guinea (PNG) and southwest of Manus Island (Rosenthal et al., 2018) (Figure 1). Site U1486 (2.37°S, 144.60°E, 1,332 m) on the northern slope of the Manus Basin is located ~25 km to the southwest and 458 m deeper than Site U1487 (2.33°S, 144.82°E, 874 m). Both sites receive large detrital contributions from the Sepik and Ramu Rivers, which drain the highlands of PNG into the Bismarck Sea, thus supporting relatively high sedimentation rates. Site U1487 is bathed by modified Antarctic Intermediate Water (mAAIW), which enters the Bismarck Sea through the Vitiaz Strait from the east and flows to the northwest (Tsuchiya, 1991). Site U1486 is bathed by modified Upper Pacific Deep Water characterized by higher salinity, lower oxygen and higher nutrients than the mAAIW (Tsuchiya, 1991; Wyrki, 1961). Present bottom water temperatures at Sites U1487 and U1486 are ~5 and 3.4°C, and salinities are 34.5 and 34.6, respectively (Figure 1, Table S1 in Supporting Information S1).

2.2. Analytical Methods

U1486 was sampled on the splice at 20 cm intervals except between depths 8.8–11.0 m and 23.7–24.5 m which were sampled at 5 cm intervals. Site U1487, with a lower sedimentation rate, was sampled on the splice at 5 cm intervals in the top 2.5 m, and at 10 cm intervals between 2.5 and 9.0 m. These samples (~30 cm³ volume, 2 cm width) were washed and picked for benthic foraminifera from the >212 μm fraction.

2.2.1. Isotope Analysis

Well-preserved benthic foraminifera, 2–3 tests per sample, were processed and analyzed for $\delta^{18}\text{O}$ and $\delta^{13}\text{C}$ with mass spectrometers using carbonate prep inlet devices. U1486 samples, alternating by depth between *Cibicidoides mundulus* and *P. wuellerstorfi*, were analyzed at the Rutgers University Stable Isotope Lab using a Micromass Optima. U1487 samples, *P. wuellerstorfi*, were analyzed at the Lamont Doherty Earth Observatory using a Thermo DeltaV+ with a Kiel IV carbonate reaction device. Analysis of in-house laboratory reference materials at both labs yielded 1-sigma standard deviations of 0.09‰ or better for $\delta^{18}\text{O}$, and 0.05‰ or better for $\delta^{13}\text{C}$.

2.2.2. Trace Element Analysis

Benthic foraminifera for trace element analysis were selected from the same samples used for isotope analysis from the >212 μm fraction. For all *P. wuellerstorfi* trace element analysis, glassy, well-formed tests were selected to be used (Rae et al., 2011). Generally, 2–6 tests provided sample weights of 200–400 μg for trace element processing; however, some samples with small tests required up to 11 foraminifera. Some samples with few glassy, well-formed tests had sample weights as low as 150 μg , and samples lacking enough glassy well-formed tests were skipped. *U. peregrina* for trace elements analysis were selected from morphotypes A, B, and/or C, as described in Stirpe et al. (2021), who report no consistent pattern or offset in Mg/Ca ratios versus temperature between these morphotypes. Generally, 3–15 tests provided sample weights of 160–450 μg for trace element processing. All tests were sonicated for 1 min in double distilled water, gently cracked open between glass slides to expose chamber interiors, and checked under an optical microscope to remove, when possible, potentially contaminating material such as pyrite. Samples were processed using the modified boron free “Cd cleaning” procedures for clay, reductive, and oxidative cleaning, followed by a 0.001 N nitric acid rinse (Rosenthal et al., 2004). After dissolution of the cleaned test calcite in 100 μl of 0.065 N nitric acid followed by

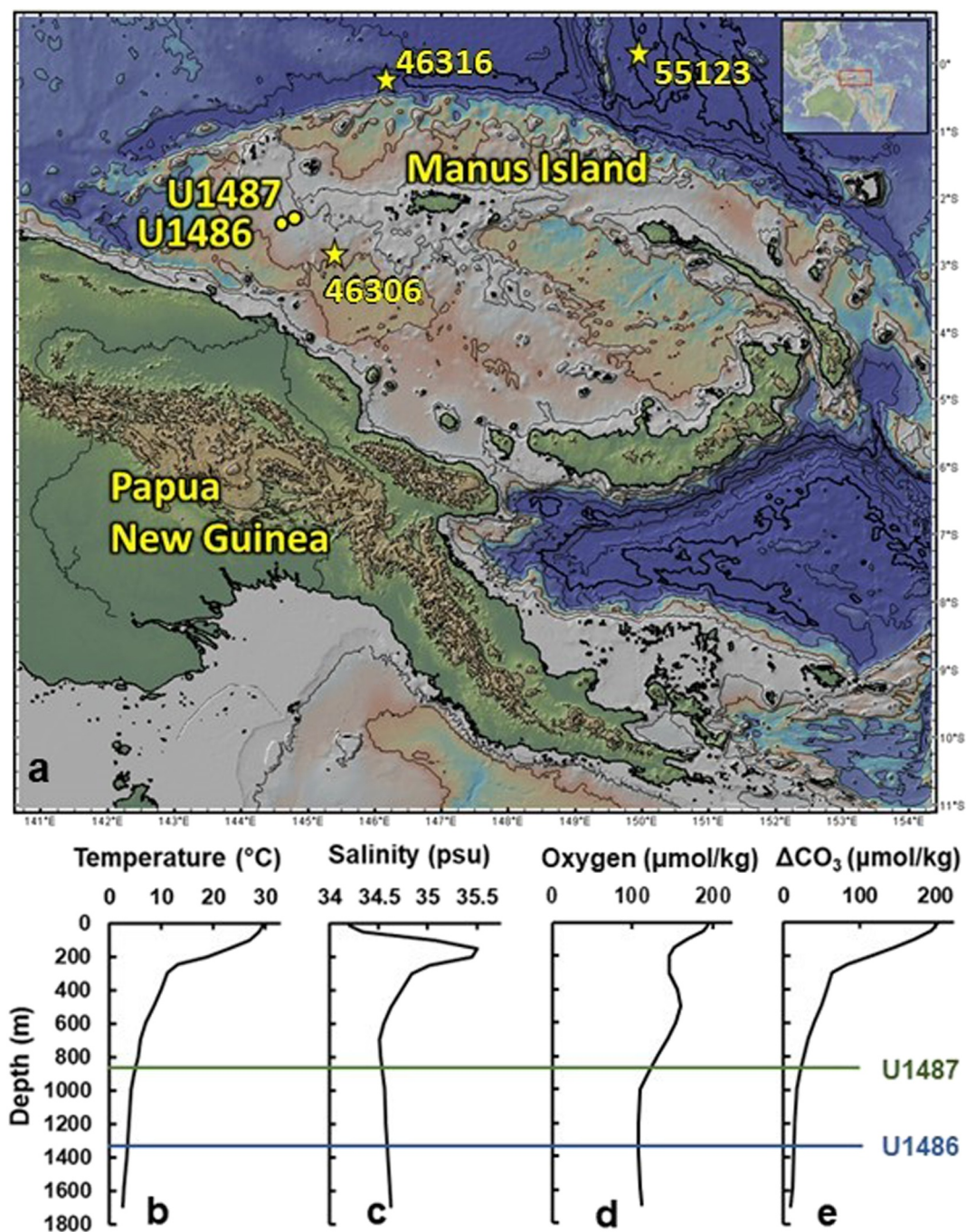


Figure 1. Bathymetry of the study region and hydrographic profiles. (a) Sites U1486 and U1487 indicated by yellow dots and cast locations by yellow stars. Sepik and Ramu Rivers (black lines) empty into the Bismarck Sea southwest of Manus Island. Figure made with GeoMapApp (www.geomapapp.org/) CC BY/CC BY (Ryan et al., 2009). Profile data from GLODAPv2.2020 (Olsen et al., 2019, 2020) were accessed through Ocean Data View (ODV) (Schlitzer, 2018). Hydrographic profiles from ODV 46306 near the study sites are of (b) temperature, (c) salinity, (d) oxygen and (e) derived carbonate saturation state (ΔCO_3). Lines on profiles are at depths of U1487 (green, 874 m) and U1486 (blue, 1,332 m). Hydrographic data were interpolated to U1486 and U1487 site depths and used to find ΔCO_3 with respect to calcite using CO2SYS.v3 (Sharp et al., 2020). Data from ODV 46316 and 55123 show the modern consistency between the study sites and the western equatorial Pacific (Text S1 and Table S1 in Supporting Information S1).

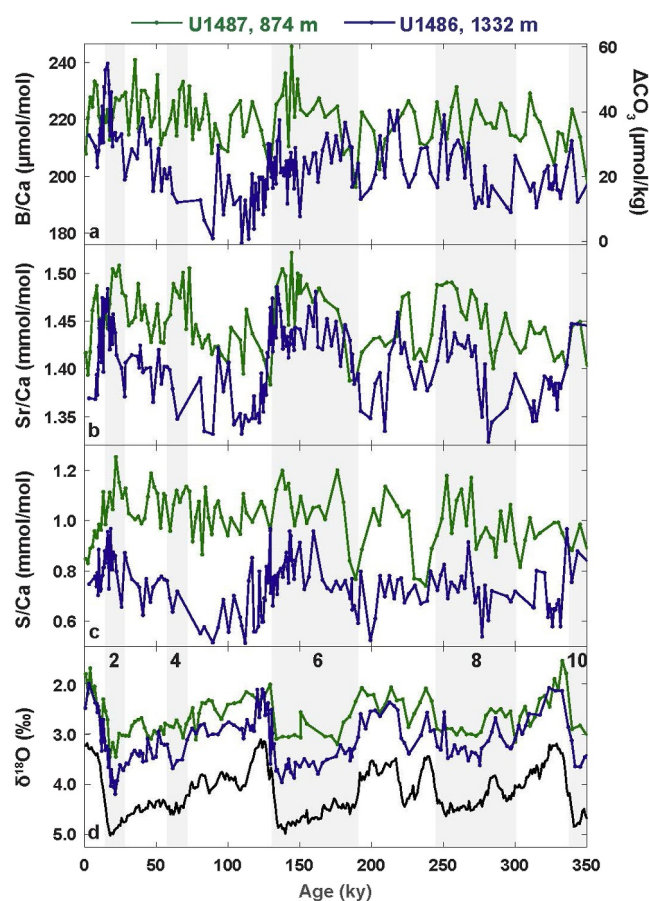


Figure 2. U1487 (green) and U1486 (blue) Boron/Calcium, Strontium/Calcium, and Sulfur/Calcium records from *P. wuellerstorfi*, with benthic $\delta^{18}\text{O}$ records. (a) B/Ca and derived ΔCO_3 using the global calibration of Yu and Elderfield (2007), $\text{B/Ca} = 1.14 \times \Delta\text{CO}_3 + 177.1$. (b) Sr/Ca. (c) S/Ca. (d) Benthic $\delta^{18}\text{O}$ records from U1487 (green), U1486 (blue, Lambert et al., 2023) and the LR04 stack (black) (Lisiecki & Raymo, 2005). Age models for U1486 and U1487 were constructed by matching benthic oxygen isotopes to LR04. Vertical gray bars mark glacial intervals identified by marine isotope stage (Lisiecki & Raymo, 2005).

centrifugation, 90 μl of solution was removed and added to 350 μl of 0.5 N nitric acid. Analysis was run on an Element XR at the Rutgers Inorganic Analytical Laboratory following the Rosenthal et al. (1999) method and modified for boron analysis with the addition of anhydrous ammonia gas (Babila et al., 2014). Relative standard deviations for B/Ca at 163 and 243 $\mu\text{mol/mol}$ are 3.3% and 2.8%, respectively; for Sr/Ca at 0.96 mmol/mol, 0.4%; for S/Ca at 4.0 mmol/mol, 1.5%; and for Mg/Ca at 1.4 mmol/mol, 0.5%. See Text S2 and Table S2 in Supporting Information S1 for consistency values, natural variability of replicates, and monitoring for cleaning, non-temperature effects, and outliers.

2.3. Age Models

The published age model for U1486 uses a core-top AMS ^{14}C date and alignment of U1486 XRF records with those from nearby site MD05-2920, which is bound by 10 AMS ^{14}C dates (Lambert et al., 2022; Tachikawa et al., 2011). The benthic $\delta^{18}\text{O}$ U1486 record beyond the range of radio carbon dating was aligned to the LR04 benthic stack (Lambert et al., 2023; Lisiecki & Raymo, 2005) (Figure 2). The U1487 age model is bound to U1486 at four depths, where sharp peaks in magnetic susceptibility and troughs in L^* reflectance are inferred to be ash layers deposited directly at both sites (Rosenthal et al., 2018). The benthic $\delta^{18}\text{O}$ U1487 was also aligned to the LR04 benthic stack (Text S3, Figures S1–S3, and Table S3 in Supporting Information S1). The U1486 sedimentation rate averages 7.3 cm/ky over the last 350 ky while at U1487 the mean rate is 2.5 cm/ky. The generally coarser particle size and lower sedimentation rate at U1487 compared with U1486 suggests greater winnowing at the shallower site (Rosenthal et al., 2018). The 20 cm sampling interval at U1486 provides resolution of 2–5 ky, and the 5 cm sampling interval, 0.5–1.2 ky resolution. At U1487, the 10 cm interval yields 3.0–5.6 ky resolution and the 5 cm interval yields 1.5–2.8 ky resolution.

3. Results

Benthic foraminiferal B/Ca, Sr/Ca, and S/Ca records from U1486 and U1487 covary with benthic $\delta^{18}\text{O}$ records from the same cores, showing G-IG variability (Figure 2). The $\delta^{18}\text{O}$ records at U1486 and U1487 show less offset during terminations and early interglacial intervals, and more offset during glacial periods, suggesting a greater difference between water at intermediate

and deeper depths during glacials. This offset pattern is also reflected in the element ratio records. At U1486, B/Ca is generally higher during glacial intervals and lower during interglacials. Also, U1486 B/Ca tends to increase toward the end of glacial periods, reaching maxima at Terminations III and II, and spiking to a maximum value of 230 $\mu\text{mol/mol}$ at the last deglaciation. In contrast, G-IG B/Ca variability at shallower site U1487 is muted, changing between 230 and 200 $\mu\text{mol/mol}$ and lacking the abrupt late deglaciation maxima observed at U1486.

Interestingly, the Sr/Ca records at both sites covary with the $\delta^{18}\text{O}$ records more closely than either B/Ca or S/Ca. Sr/Ca at U1486 showed deglacial spikes at all three terminations without similar concurrent abrupt maxima at U1487. During Terminations I and II, Sr/Ca values at the sites are not offset. The G-IG variability in S/Ca at the two sites showed similar variability to B/Ca. The only discernible S/Ca spike appears in U1486 during Termination I. Notably, all three elemental ratios exhibit a weak increasing trend at U1487 over the 350 ky record. We also note that the infaunal *U. peregrina* Sr/Ca records at U1486 and U1487 show similar covariance with Sr/Ca in the epifaunal *P. wuellerstorfi* (Figures 3a and 3b).

The Mg/Ca records from *U. peregrina* covary with $\delta^{18}\text{O}$ records during marine isotope stage (MIS) 9 when both sites have maximum Mg/Ca and during MIS 2 and 3 when they have minimum Mg/Ca before rising to modern values. However, at both sites during MIS 6 Mg/Ca is relatively high, and in MIS 8 the amplitude of the G-IG

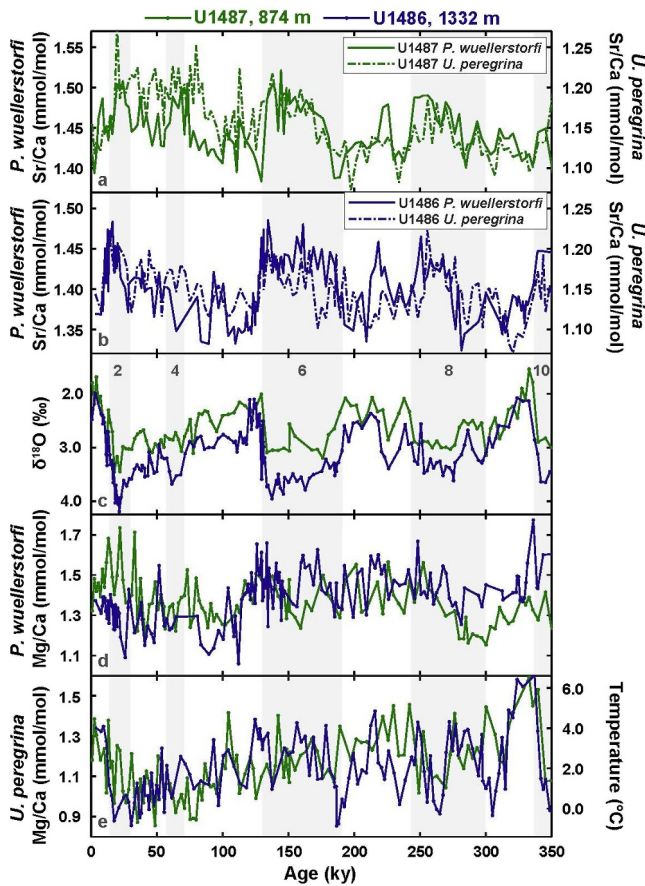


Figure 3. U1487 (green) and U1486 (blue) Strontium/Calcium and Magnesium/Calcium records from epifaunal *P. wuellerstorfi* and infaunal *U. peregrina* with benthic $\delta^{18}\text{O}$ records. (a) U1487 and (b) U1486 show Sr/Ca from *P. wuellerstorfi* (solid line, left axis) and *U. peregrina* (dashed line, right axis). Note that the left axis is shifted between (a) and (b); the right axis is not. (c) U1487 (green) and U1486 (blue) benthic $\delta^{18}\text{O}$ records. Vertical gray bars indicate glacials identified by marine isotope stage number (Lisiecki & Raymo, 2005). (d) *P. wuellerstorfi* Mg/Ca records from U1487 (green) and U1486 (blue). (e) *U. peregrina* Mg/Ca records (left axis) from U1487 (green) and U1486 (blue) and derived bottom water temperature (BWT) (right axis) using $\text{Mg/Ca} = 0.1 \times \text{BWT} + 0.94$ (Elderfield et al., 2012, adjusted for this study per Section 4.1).

Bottom water temperatures for U1486 and U1487 were estimated from Mg/Ca in *U. peregrina* using the calibration of $\text{Mg/Ca} = 0.1 \times \text{BWT} + 0.94$, based on (Elderfield et al., 2010) after adjustment for a 10% offset since we used an additional reductive cleaning step (Rosenthal et al., 2004). At both U1486 and U1487, the temperatures (Figure 3e, right axis) range from ~ 0 – 6.5°C , and have minimum temperatures in MIS 2 and 3 before rising to present values of about 4°C in the late Holocene, consistent with present bottom water temperatures (3.4 , and $\sim 5^\circ\text{C}$, respectively) and within the estimated uncertainty ($\pm 1^\circ\text{C}$) of the calibration (Elderfield et al., 2012). Both sites generally covary with maximum temperatures near 6.5°C in MIS 9; during MIS 6, temperatures rise from a low at the beginning of the glacial to around 3°C before decreasing through MIS 5 into glacial MIS 4. An exception is around Termination II when U1486 temperatures rise to around 4°C , while U1487 temperatures remain around 2°C .

cycles are quite different (Figures 3c and 3e), and there is little correlation between the Mg/Ca and $\delta^{18}\text{O}$ records (U1486, $r^2 = 0.18$; U1487, $r^2 = 0.14$). Unlike $\delta^{18}\text{O}$, the Mg/Ca records from *U. peregrina* do not show a variable G-IG offset between the shallow and deeper sites. The range of *U. peregrina* Mg/Ca for both sites is similar (0.85–1.6 mmol/mol).

The Mg/Ca records from *P. wuellerstorfi* show little G-IG covariance with Mg/Ca records from *U. peregrina* or with $\delta^{18}\text{O}$ records, with an overall range for *P. wuellerstorfi* Mg/Ca of ~ 0.6 mmol/mol at both sites (1.1–1.7 mmol/mol, Figures 3c–3e). At U1487, the highest Mg/Ca is in recent glacial cycles and lowest Mg/Ca in MIS 8 and 9. At U1486, Mg/Ca is higher in MIS 6 and older, while more recent Mg/Ca is lower, reaching a record minimum in MIS 5.

4. Discussion

The Sr/Ca and S/Ca records from U1486 and U1487 covary with B/Ca (Figures 2a,b,c), suggesting that Sr/Ca and S/Ca in test calcite are also primarily driven by changes in ΔCO_3 and possibly may be used to supplement B/Ca as proxies for ΔCO_3 (van Dijk et al., 2017; Yu, Elderfield, et al., 2014). By comparing these records with ΔCO_3 estimates derived from B/Ca measured concurrently on *P. wuellerstorfi*, and with BWT estimates derived from *U. peregrina* Mg/Ca, we assessed the effects of ΔCO_3 and temperature on Sr/Ca, S/Ca, and Mg/Ca.

4.1. ΔCO_3 and Temperature Records

We have generated down-core ΔCO_3 records for U1486 and U1487 (Figure 2a, right axis) from the B/Ca *P. wuellerstorfi* record using the calibration $\text{B/Ca} = (1.14 \pm 0.048) \times \Delta\text{CO}_3 + (177.1 \pm 1.41)$ (Yu & Elderfield, 2007). Throughout the past 350 ky, the ΔCO_3 variability derived from *P. wuellerstorfi* B/Ca ($\Delta\text{CO}_{3-\text{B/Ca}}$) at U1486 ranged from 0 to $55 \mu\text{mol/kg}$. At U1487, the upper range is similar but the lower range rarely goes below $20 \mu\text{mol/kg}$. The mean $\Delta\text{CO}_{3-\text{B/Ca}}$ over 350 ky at U1486 ($23 \mu\text{mol/kg}$) is less than that at U1487 ($38 \mu\text{mol/kg}$) by $15 \mu\text{mol/kg}$. The $\Delta\text{CO}_{3-\text{B/Ca}}$ at U1486 is usually lower, but with a prominent exception at the end of MIS 2 and concurrent with Heinrich Stadial 1 (HS1, 18–14 ky) when the $\Delta\text{CO}_{3-\text{B/Ca}}$ at U1486 is $\sim 12 \mu\text{mol/kg}$ higher than at U1487. U1486 $\Delta\text{CO}_{3-\text{B/Ca}}$ has greater amplitude in G-IG changes, tends to increase toward the end of glacials, and decreases to a record minimum during interglacial MIS 5. U1487 $\Delta\text{CO}_{3-\text{B/Ca}}$ shows less G-IG amplitude and an overall trend toward increasing $\Delta\text{CO}_{3-\text{B/Ca}}$ over the 350 ky period.

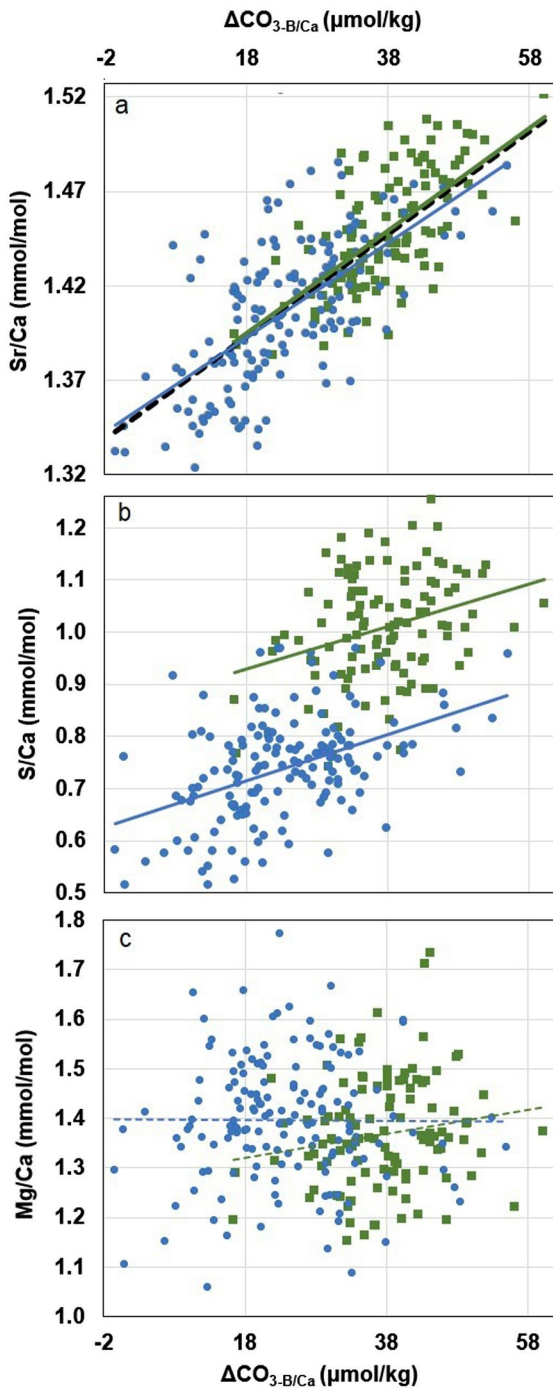


Figure 4. Regressions of Strontium/Calcium, Sulfur/Calcium, and Magnesium/Calcium with $\Delta\text{CO}_{3\text{-B/Ca}}$ in *P. wuellerstorfi* at U1486 (blue dots) and U1487 (green squares). (a) Sr/Ca: regression lines for U1486 (solid blue, $\text{Sr/Ca} = 0.0025 \times (\Delta\text{CO}_{3\text{-B/Ca}}) + 1.35$, $r^2 = 0.44$); U1487 (solid green, $\text{Sr/Ca} = 0.0027 \times (\Delta\text{CO}_{3\text{-B/Ca}}) + 1.35$, $r^2 = 0.43$); and both sites combined (dashed black, $\text{Sr/Ca} = 0.0027 \times (\Delta\text{CO}_{3\text{-B/Ca}}) + 1.34$, $r^2 = 0.58$). (b) S/Ca and regression lines for U1486 (solid blue, $\text{S/Ca} = 0.0044 \times (\Delta\text{CO}_{3\text{-B/Ca}}) + 0.64$, $r^2 = 0.19$) and U1487 (solid green, $\text{S/Ca} = 0.0041 \times (\Delta\text{CO}_{3\text{-B/Ca}}) + 0.86$, $r^2 = 0.09$) showing an offset in S/Ca between the regression lines. (c) Mg/Ca from *P. wuellerstorfi* shows no apparent correlation with $\Delta\text{CO}_{3\text{-B/Ca}}$ at either U1486 (dashed blue, $r^2 = 0.00$) or U1487 (dashed green, $r^2 = 0.03$).

4.2. ΔCO_3 and Temperature Effects on Strontium/Calcium

Strontium/Calcium correlated with $\Delta\text{CO}_{3\text{-B/Ca}}$ at U1486 and U1487 ($r^2 = 0.44, 0.43$, respectively, Figure 4a). The regressions from both sites are indistinguishable, yielding almost identical sensitivity of Sr/Ca to ΔCO_3 and offsets. The lack of an offset in Sr/Ca between the two sites allows us to use data from both sites for a combined linear down-core calibration ($n = 273$, $r^2 = 0.58$, Figure 4a, Table S4 in Supporting Information S1, reported errors are 1-sigma standard deviation):

$$\text{Sr/Ca} = (0.0027 \pm 0.0001) \times \Delta\text{CO}_{3\text{-B/Ca}} + (1.344 \pm 0.004) \quad (1)$$

The bivariate regression from the combined down-core ΔCO_3 and temperature data yields a sensitivity to ΔCO_3 (0.0027 ± 0.0002) and an intercept (1.35 ± 0.01) statistically indistinguishable from those in the univariate regression (Table S4, S5 in Supporting Information S1). The inclusion of temperature, derived from *U. peregrina* Mg/Ca, in the linear regression model does not significantly change the model nor improve the correlation, giving evidence that temperature does not influence the distribution coefficient of Sr/Ca into calcite. As a further test, we used the regression from U1486, $\text{Sr/Ca} = (0.0025 \pm 0.0002) \times \Delta\text{CO}_{3\text{-B/Ca}} + (1.35 \pm 0.01)$; $n = 158$, $r^2 = 0.44$ (Table S4 in Supporting Information S1) to predict Sr/Ca values at U1487 from the paired B/Ca measurements. The test yields a close agreement between the measured Sr/Ca and the predicted Sr/Ca (Figure S4a in Supporting Information S1). Additionally, it has been suggested that Sr may be linked to Mg through defects in the crystalline lattice as the cations both replace Ca^{2+} in calcite, and that the Sr/Ca partition coefficient is kinetically controlled by the calcite Mg content (Carpenter & Lohmann, 1992). We tested a possible kinetic effect of Mg/Ca on Sr/Ca by regressing to $\Delta\text{CO}_{3\text{-B/Ca}}$ and Mg/Ca from the same *P. wuellerstorfi* samples. This combined bivariate regression also does not significantly change the sensitivity of Sr/Ca to ΔCO_3 (0.0027 ± 0.0001 , Table S6 in Supporting Information S1), giving evidence that there is no significant kinetic Mg/Ca effect on Sr/Ca in calcite. For additional evidence, at each site Sr/Ca from *U. peregrina* covaries with Sr/Ca from *P. wuellerstorfi*, while Mg/Ca from the two species does not (Figures 3 and 5).

4.3. ΔCO_3 and Temperature Effects on Sulfur/Calcium

Sulfur/Calcium in *P. wuellerstorfi*, despite the visual similarity, shows little correlation with $\Delta\text{CO}_{3\text{-B/Ca}}$ at U1486, and even less so at U1487 (Figure 4b). Additionally, the regressions for S/Ca from U1486 and U1487 are offset, suggesting the possibility of secondary effects on S/Ca, such as temperature (Berry, 1998) or the Mg content of the *P. wuellerstorfi* shells (van Dijk et al., 2017). Additionally, since the temperature records of the two sites are the same within the calibration uncertainty and yet the $\delta^{18}\text{O}$ records are offset, salinity may have a secondary influence.

As with the single linear regressions of S/Ca against ΔCO_3 , the bivariate regressions including temperature show little correlation at U1486 ($r^2 = 0.15$, $n = 89$) and slightly better correlation at U1487 ($r^2 = 0.25$, $n = 103$). When the suites of data from the two sites for the interval 150–0 ky are combined into one bivariate regression, we obtain the following calibration ($n = 92$, $r^2 = 0.53$):

$$\text{S/Ca} = (-0.020 \pm 0.010) \times \text{BWT} + (0.011 \pm 0.001) \times \Delta\text{CO}_{3\text{-B/Ca}} + (0.60 \pm 0.04) \quad (2)$$

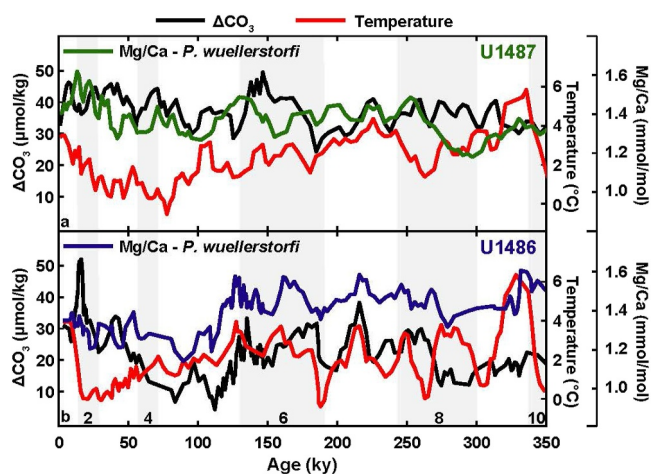


Figure 5. Covariation of Mg/Ca from *P. wuellerstorfi* with ΔCO_3 derived using B/Ca from *P. wuellerstorfi* (black) and temperature derived from *U. peregrina* Mg/Ca (red) at (a) U1487 (green) and (b) U1486 (blue). ΔCO_3 estimates derived using $\text{B/Ca} = 1.14 \times \Delta\text{CO}_3 + 177.1$ (Yu & Elderfield, 2007). Temperature estimates derived using $\text{Mg/Ca} = 0.1 \times \text{bottom water temperature} + 0.94$ (Elderfield et al., 2012, adjusted for this study per Section 4.1). All records are smoothed using a three-point running mean to show trends (data, Figures 2 and 3). Vertical gray bars indicate glacials identified by marine isotope stage number (Lisiecki & Raymo, 2005).

which explains 53% of the variability. Despite the insignificant temperature difference between the sites, including the *U. peregrina*-derived temperature in the combined bivariate regression increases the ability of the model to explain the S/Ca variability at U1486 and U1487 (Tables S4 and S5 in Supporting Information S1). To test the above regression that uses data from both sites (for the interval 150–0 ky), we use it to predict S/Ca from B/Ca derived ΔCO_3 from *P. wuellerstorfi* and Mg/Ca derived temperature from *U. peregrina* from each site (for the interval 350–150 ky) and compare it with the S/Ca from the same analysis derived from *P. wuellerstorfi* at that site (Figures S2b and S2c in Supporting Information S1). The amplitude, offset, and progression of the predicted S/Ca (350–150 ky) are similar to those of the S/Ca data at both U1486 and U1487. These observations support a possible additional temperature effect on the distribution coefficient of S/Ca. The S/Ca bivariate regressions at U1486 and U1487 and the regression combining both sites have negative coefficients for temperature and positive coefficients for ΔCO_3 indicating that temperature and ΔCO_3 have opposing effects on S/Ca. From this we arrive at a contrasting conclusion from that of van Dijk et al. (2017) and suggest that S/Ca would not make a good proxy for ΔCO_3 reconstruction.

It has been suggested that Mg and S are mechanistically linked during calcification as higher S and Mg concentrations co-occur in bands in benthic foraminiferal calcite (van Dijk et al., 2017). Thus, we also tested for a Mg/Ca effect on S/Ca by regressing to $\Delta\text{CO}_{3-\text{B/Ca}}$ and Mg/Ca from *P. wuellerstorfi* for the interval 150–0 ky, obtaining the following calibration ($n = 149$, $r^2 = 0.53$):

$$\text{S/Ca} = (0.38 \pm 0.08) \times \text{Mg/Ca} + (0.0093 \pm 0.0008) \times \Delta\text{CO}_{3-\text{B/Ca}} + (0.07 \pm 0.11) \quad (3)$$

which also explains 53% of the variability. As before, we use this regression to predict S/Ca from derived ΔCO_3 and Mg/Ca from *P. wuellerstorfi* from each site for the interval 350–150 ky and compare it with the S/Ca (Figure S5 in Supporting Information S1). The amplitude, offset, and progression of the predicted S/Ca (350–150 ky) using Mg/Ca are similar to those of the S/Ca data at both U1486 and U1487. At this time, using the records in this study, we cannot determine whether temperature or a mechanistic link to Mg/Ca influences S/Ca in the foraminiferal calcite. However, since Mg/Ca in *P. wuellerstorfi* is understood to be affected by both ΔCO_3 and temperature, and assuming the relationships with ΔCO_3 and temperature remain the same in the past, there is a potential for using sulfur in foraminiferal calcite to reconstruct a long-term (e.g., Cenozoic) record of sulfate in the ocean. Using paired B/Ca and Mg/Ca from *P. wuellerstorfi* would eliminate the need for additionally measuring Mg/Ca from *U. peregrina* for temperature.

4.4. ΔCO_3 and Temperature Effects on Mg/Ca

Magnesium/Calcium in the epifaunal *P. wuellerstorfi* can be affected by changes in bottom water ΔCO_3 in addition to temperature (Yu & Elderfield, 2008). At low ΔCO_3 (<30 $\mu\text{mol/kg}$) and low temperatures (<3°C), less Mg is incorporated into *P. wuellerstorfi* test calcite than would be expected from a global temperature calibration (Martin et al., 2002). At both U1486 and U1487, the Mg/Ca in *P. wuellerstorfi* shows stronger covariation with changes in the $\Delta\text{CO}_{3-\text{B/Ca}}$ record than with changes in temperature derived from *U. peregrina* Mg/Ca. This suggests that control of Mg/Ca in *P. wuellerstorfi* calcite is dominated by ΔCO_3 at these sites, although the correlation between *P. wuellerstorfi* Mg/Ca and $\Delta\text{CO}_{3-\text{B/Ca}}$ is not statistically significant (Figure 4c). The saturation state and temperature at times oppose each other, and at other times work together. To make the temporally varying relationships noted above more apparent, the records in Figure 5 are smoothed using a three-point running mean. The effect of opposing forcing is clearly seen after ~75 ky when at U1486 the temperature decreases while the ΔCO_3 increases: the Mg/Ca from *P. wuellerstorfi* remains at moderate levels (Figure 5b). At U1487 after ~75 ky, the effects of ΔCO_3 and temperature work together:

when temperatures rise, ΔCO_3 is also high, and the Mg/Ca *P. wuellerstorfi* record reaches a maximum in the 350 ky record (Figure 5a). At both U1486 and U1487, the *P. wuellerstorfi* Mg/Ca records show variability, little change in amplitude over G-IG cycles, and a tendency to follow ΔCO_3 over temperature on G-IG time scales. Opposing forcing by ΔCO_3 and temperature in the western equatorial Pacific mutes the G-IG Mg/Ca changes and thus complicates the reconstruction of bottom water temperatures from *P. wuellerstorfi* Mg/Ca. These results are distinct from those in the North Atlantic, where variations in ΔCO_3 and temperature work in concert to generate an apparent higher sensitivity of Mg/Ca to temperature (Ford et al., 2016; Sosdian & Rosenthal, 2009, 2010).

Bivariate regressions for *P. wuellerstorfi* Mg/Ca from *U. peregrina*-derived temperature and $\Delta\text{CO}_{3-B/\text{Ca}}$ also yield no correlation (U1486, $r^2 = 0.06$; U1487 $r^2 = 0.02$; U1486 and U1487 combined, $r^2 = 0.01$). However, general trends over the entire 350 ky records seem to follow forcing by ΔCO_3 (Figure 5). Both the *P. wuellerstorfi* Mg/Ca and the $\Delta\text{CO}_{3-B/\text{Ca}}$ records at U1487 have broad increasing trends. At U1486, the lowest *P. wuellerstorfi* Mg/Ca ratios are during interglacial MIS 5 when $\Delta\text{CO}_{3-B/\text{Ca}}$ is also at a minimum. At U1486 and U1487 in the western equatorial Pacific, ΔCO_3 and temperature have an opposing influence on the variability of Mg/Ca in epifaunal *P. wuellerstorfi* calcite, and the influence of ΔCO_3 is apparently stronger.

5. Application of Benthic Foraminiferal Sr/Ca as a Proxy for ΔCO_3

5.1. Core-Tops Regressions for Sr/Ca

Yu and Elderfield et al. (2014) regressed benthic foraminiferal Sr/Ca to ΔCO_3 and report significant offsets in both down-core and core-top calibrations from Atlantic, Pacific and Indian basins. We add new paired Sr/Ca and ΔCO_3 core-top data ($n = 165$) to the published core-top data of Yu and Elderfield et al. (2014) and Lo Giudice Cappelli et al. (2015). The regressions from the combined core-top data show variable sensitivities for *P. wuellerstorfi* in the Atlantic, Pacific, and Indian Oceans, and for *Cibicides* spp. (*C. mundulus*, also known as *C. kullenbergi* and *C. pachyderma*) in the Atlantic and Indo-Pacific, consistent with previously published calibrations (Figure 6, Table 1). The species offset in the Atlantic between *P. wuellerstorfi* and the *Cibicides* spp. is 0.10 mmol/mol (Figure 6c and Table 1).

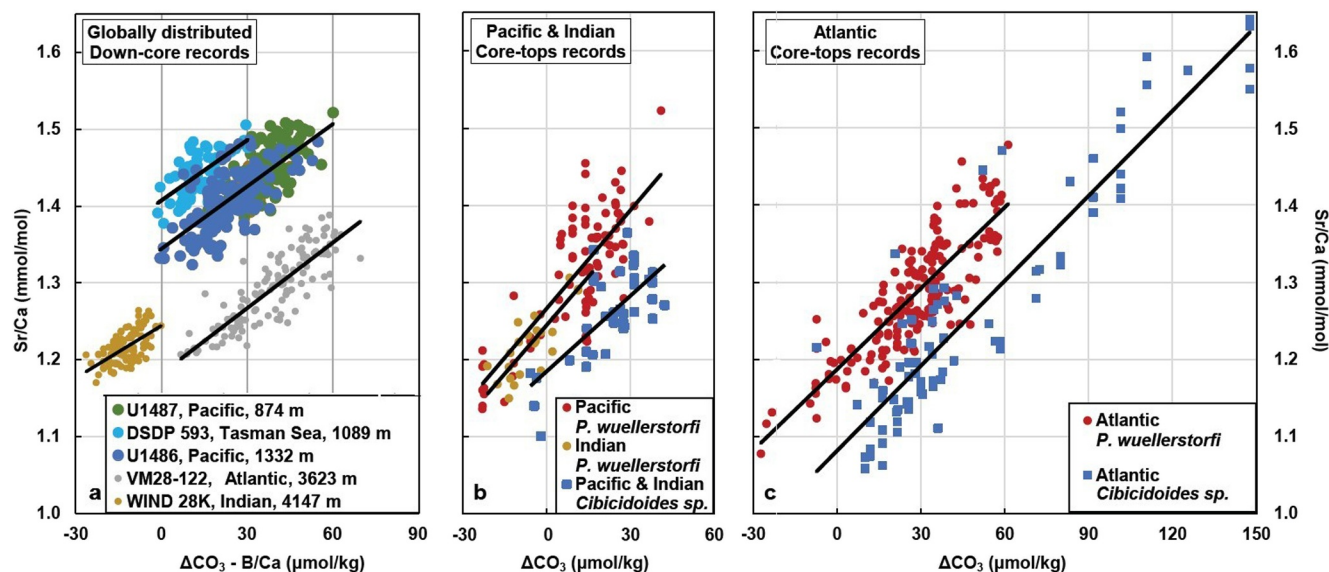


Figure 6. Regressions of down-core paired Sr/Ca to B/Ca-derived ΔCO_3 and regressions of core-top paired Sr/Ca to modern ΔCO_3 . (a) Down-core regressions of Sr/Ca to ΔCO_3 derived from B/Ca from various ocean basins show similar sensitivities but significant offsets (Table 2). U1486 (dark blue), U1487 (green), and DSDP 593 (light blue) are from this study. DSDP 593 adds new Sr/Ca data that is paired to B/Ca data from Elmore et al. (2015). VM28-122 (gray), and WIND 28K (light brown) are from Yu and Elderfield et al. (2014). All down-core records are from *P. wuellerstorfi*. For (b) and (c) we add paired Sr/Ca from core tops and modern ΔCO_3 data from GEOSECS (Bainbridge, 1981; Broecker et al., 1982; Weiss et al., 1983) of WOCE (Chapman, 1998) to previously published core-top records from Yu and Elderfield et al. (2014), and Lo Giudice Cappelli et al. (2015). (b) Separate Pacific and Indian core-top regressions of Sr/Ca to ΔCO_3 for *P. wuellerstorfi* and a combined Indo-Pacific regression for *Cibicides* spp. (Table 1). (c) Atlantic core-top regressions of Sr/Ca to ΔCO_3 for *P. wuellerstorfi* and *Cibicides* spp. (Table 1).

Table 1
Regressions From Paired Core-Top Strontium/Calcium and Modern ΔCO_3 Data for *P. wuellerstorfi* and *Cibicidoides* spp. (*Cib. spp.*) (Figures 6b and 6c Core-Top Data From This Study, Lo Giudice Cappelli et al., 2015; Yu, Elderfield, et al., 2014)

| | |
|-----------------------------------|---|
| Atlantic, <i>P. wuellerstorfi</i> | $\text{Sr/Ca} = (0.0035 \pm 0.0002) \times \Delta\text{CO}_3 + (1.187 \pm 0.006)$; $n = 185$, $r^2 = 0.70$ |
| Pacific, <i>P. wuellerstorfi</i> | $\text{Sr/Ca} = (0.0043 \pm 0.0004) \times \Delta\text{CO}_3 + (1.266 \pm 0.007)$; $n = 90$, $r^2 = 0.62$ |
| Indian, <i>P. wuellerstorfi</i> | $\text{Sr/Ca} = (0.0042 \pm 0.0006) \times \Delta\text{CO}_3 + (1.245 \pm 0.006)$; $n = 23$, $r^2 = 0.71$ |
| Atlantic, <i>Cib. spp.</i> | $\text{Sr/Ca} = (0.0037 \pm 0.0002) \times \Delta\text{CO}_3 + (1.082 \pm 0.011)$; $n = 83$, $r^2 = 0.85$ |
| Indo-Pacific, <i>Cib. spp.</i> | $\text{Sr/Ca} = (0.0033 \pm 0.0005) \times \Delta\text{CO}_3 + (1.185 \pm 0.014)$; $n = 38$, $r^2 = 0.51$ |

5.2. Down-Core Regressions of Sr/Ca to $\Delta\text{CO}_{3\text{-B/Ca}}$ From Globally Distributed Records

The apparently variable core-top sensitivities obtained in the different ocean basins may be an artifact of the quality of the core-top samples (e.g., not all are of modern age, geographical sample limitation) and/or of the hydrographic data. Therefore, we further explored the calibrations using a globally distributed collection of down-core paired Sr/Ca and $\Delta\text{CO}_{3\text{-B/Ca}}$ records from *P. wuellerstorfi*. We add our combined down-core data from the two Pacific sites (U1486, 1,332 m; U1487, 874 m) and new Sr/Ca data from the Tasman Sea (DSDP 593, 1,089 m) that is paired to existing down-core B/Ca data from Elmore et al. (2015), to published records from the Atlantic (VM28-122, 3,623 m) and Indian Ocean (WIND 28K, 4,147 m) from Yu and Elderfield et al. (2014) (Figure 6a). The combined U1486 and U1487 records yield a sensitivity of Sr/Ca to $\Delta\text{CO}_{3\text{-B/Ca}}$ of 0.0027 ± 0.0001 mmol/mol per $\mu\text{mol/kg}$, consistent with the sensitivities of the records from the Atlantic (0.0028 ± 0.0002), Tasman Sea (0.0026 ± 0.0004), and Indian Ocean (0.0023 ± 0.0003) within 2 SD (Table 2). In comparison, core-top calibrations of *P. wuellerstorfi* yield higher and more variable sensitivities to ΔCO_3 of 0.0035 ± 0.0002 , 0.0043 ± 0.0004 , and 0.0042 ± 0.0006 in the Atlantic, Pacific, and Indian Oceans, respectively (Table 1). As reported previously (Yu, Elderfield, et al., 2014), significant offsets in Sr/Ca are found in both the down-core and core-top records from the Atlantic, Pacific, and Indian basins (Figure 6, Tables 1 and 2). Our calibrations suggest that these offsets are not likely from a temperature difference because there is an offset between the combined U1486 and U1487 regression and the regression from DSDP 593, despite similar temperature ranges at all three sites (DSDP 593 range is 1–5°C, Elmore et al., 2015). Similarly, we excluded any influence from pressure/depth differences since the offsets do not vary according to the sites' depth (Figure 6a). Instead, the offsets in the core-top calibrations between the Atlantic, Pacific, and Indian basins (Figures 6b and 6c) are consistent with the pattern of the offsets in the down-core records, possibly indicating that the basin to basin offsets are persistent for at least the last three G-IG cycles. Given the offset in the Atlantic core-top regressions of Sr/Ca to ΔCO_3 between *P. wuellerstorfi* and *Cibicidoides* spp. (Figure 6c), it may be the case that *P. wuellerstorfi* from different ocean basins, although morphologically the same, are chemically different, and this difference persisted at least for the past few hundred thousand years.

Table 2
Regressions for a Globally Distributed Collection of Paired Down-Core Records of Sr/Ca and B/Ca Derived ΔCO_3 From *P. wuellerstorfi*

| | |
|--------------------------|---|
| Atlantic, VM28-122 | $\text{Sr/Ca} = (0.0028 \pm 0.0002) \times \Delta\text{CO}_{3\text{-B/Ca}} + (1.182 \pm 0.006)$; $n = 123$, $r^2 = 0.73$ |
| Pacific, U1487 and U1486 | $\text{Sr/Ca} = (0.0027 \pm 0.0001) \times \Delta\text{CO}_{3\text{-B/Ca}} + (1.344 \pm 0.004)$; $n = 273$, $r^2 = 0.58$ |
| Tasman Sea, DSDP 593 | $\text{Sr/Ca} = (0.0026 \pm 0.0004) \times \Delta\text{CO}_{3\text{-B/Ca}} + (1.407 \pm 0.006)$; $n = 68$, $r^2 = 0.39$ |
| Indian, WIND 28K | $\text{Sr/Ca} = (0.0023 \pm 0.0003) \times \Delta\text{CO}_{3\text{-B/Ca}} + (1.244 \pm 0.004)$; $n = 106$, $r^2 = 0.38$ |

Note. See Figure 6, Data Set S3 in Supporting Information S1, Elmore et al. (2015), Yu, Elderfield, et al. (2014).

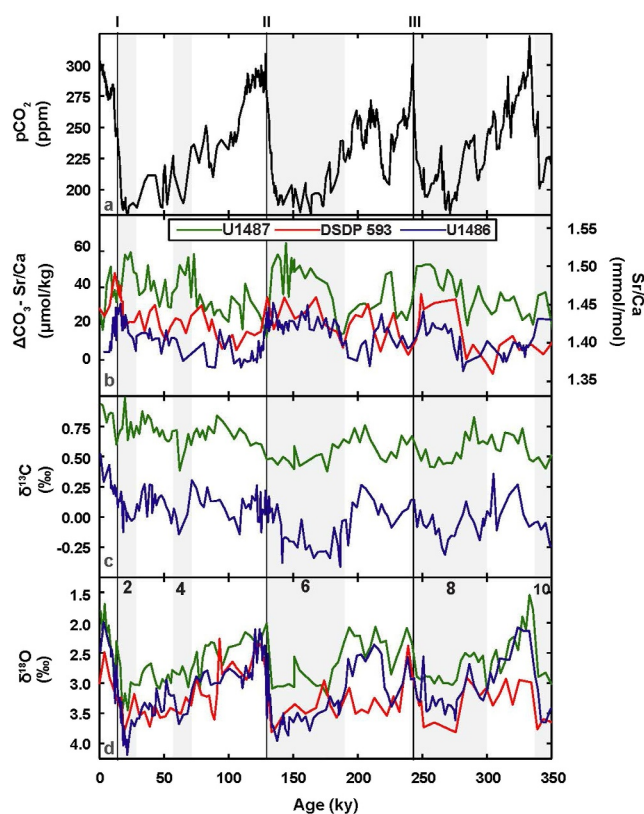


Figure 7. Evidence for deep ocean release of carbon dioxide at three glacial terminations inferred from multiple proxies from U1487 (green), DSDP 593 (red), and U1486 (blue). Vertical gray bars indicate glacial intervals identified by marine isotope stage number (Lisiecki & Raymo, 2005). Black vertical lines indicate Terminations I, II, and III. (a) Atmospheric $p\text{CO}_2$ record from EDC3 ice cores (Bereiter et al., 2015; Lüthi et al., 2008; Petit et al., 1999; Siegenthaler et al., 2005). (b) Intermediate and upper deep water carbonate saturation state derived from Sr/Ca records using the down-core derived upper Pacific *P. wuellerstorfi* sensitivity to ΔCO_3 , 0.00266 ± 0.00022 mmol/mol per $\mu\text{mol/kg}$, and offsets of 1.35 mmol/mol at U1487 and U1486, and 1.407 mmol/mol at DSDP 593. (c) $\delta^{13}\text{C}$ records from U1487 and U1486. (d) $\delta^{18}\text{O}$ records from U1487, DSDP 593, and U1486 (this study, Elmore et al., 2015; this study, respectively).

Since the sensitivities of the down-core records are more consistent than those from the core-tops data, we suggest that the down-core sensitivities are more reliable for use as a potential proxy for ΔCO_3 derived from Sr/Ca (Sr/Ca- ΔCO_3). Sites U1486, U1487, and DSDP 593 are bathed in intermediate water or upper deep water close to the present water mass transition (Figure 1, and see Elmore et al., 2015). We use the sensitivities from these sites, which are within 1 SD (Table 2, Table S4 in Supporting Information S1), to derive a sensitivity for upper Pacific interior waters, 0.00266 ± 0.00022 mmol/mol per $\mu\text{mol/kg}$ (the sensitivity average weighted by the correlation for Pacific combined sites U1486 and U1487, and Tasman Site DSDP 593). The offset is basin specific and so needs to be determined for each site. We use 1.35 mmol/mol for both western equatorial Pacific sites and 1.407 mmol/mol for the Tasman Sea site (Table 2, Table S4 in Supporting Information S1). The upper Pacific interior water sensitivity and site specific offsets were used to reconstruct upper Pacific interior water Sr/Ca- ΔCO_3 records from U1486, U1487, and DSDP 593 (Figure 7).

6. Paleoclimatological Implications

At present, we cannot unequivocally determine the causes for apparent inter-basin differences in the calibration of Sr/Ca versus ΔCO_3 , but the data suggest that the calibrations are constant within each basin for at least ~ 300 ky. One may wonder, however, what is the benefit of using Sr/Ca when we can instead use B/Ca as a proxy for ΔCO_3 ? First, it is easier to measure Sr/Ca when acquiring Mg/Ca data, compared to the difficult process of measuring B/Ca, due to the high potential for contamination of samples with environmental boron during lab work (Misra et al., 2014; Rae et al., 2011). Second, Sr/Ca records may add fine details of the carbonate chemistry that are not captured by the B/Ca. This can be demonstrated in the records from sites U1487 and U1486, in which spikes show up clearly in both B/Ca and Sr/Ca at Termination I, but peaks in Terminations II and III show up more clearly in the Sr/Ca (Figure 2). As with ΔCO_3 from B/Ca, a Sr/Ca- ΔCO_3 abrupt increase suggests a rapid rise in carbonate ion concentration in the water at the site depth. The timing of the U1486 Sr/Ca- ΔCO_3 peak during the last deglaciation (16–14 ky, Figure 7) coincides with the known preservation event of aragonitic pteropods in deep ocean sediments (Berger, 1977), which has been attributed to venting of carbon during the deglacial rise of atmospheric CO_2 (Naidu et al., 2014). Below we briefly discuss the implications of these records, but note that a full discussion of the paleoclimatological implications will be offered in a follow-up paper.

Like the ΔCO_3 derived from B/Ca, the Sr/Ca- ΔCO_3 is relatively high during the last glacial period as compared to the Holocene, consistent with a glacial increase in alkalinity in the Southern Ocean (Rickaby et al., 2010), and consistent with a different glacial circulation pattern in the Pacific upper overturning cell (Clementi & Sikes, 2019; Rafter et al., 2022; Ronge et al., 2015). The pattern of high Sr/Ca- ΔCO_3 during the last glacial period repeats from the three previous glacial periods (Figure 7b). High ΔCO_3 is often associated with increased ventilation and reduced carbon storage; however, although the glacial Sr/Ca- ΔCO_3 is high relative to the interglacials, glacial benthic $\delta^{13}\text{C}$ at U1486 and U1487 is depleted, indicating enhanced glacial carbon storage, with the greater offset in $\delta^{13}\text{C}$ between U1486 and U1487 during glacial intervals indicating more storage of carbon at $\sim 1,300$ m depth during glacial periods (Figure 7c). Additionally, studies inferring dissolved oxygen levels suggest that glacial ventilation was reduced in both Pacific overturning cells relative to interglacials, increasing carbon storage and deepening its location (Anderson et al., 2019; Jacobel et al., 2017). We suggest that enhanced carbon storage in glacial intervals is masked in our Sr/Ca- ΔCO_3 records by a glacial increase in alkalinity (Rickaby et al., 2010), which adds carbonate ions and buffers the seawater. Glacial Pacific upper interior waters with higher Sr/Ca- ΔCO_3 relative to water at the same depth during interglacial periods may actually be less

ventilated. The higher glacial Sr/Ca- ΔCO_3 may be a consequence of greater carbon storage, which led to higher dissolution of carbonate sediments that increased carbonate ions and thus raised ΔCO_3 . As bottom water ΔCO_3 at these sites is above the level for carbonate dissolution ($>0 \mu\text{mol/kg}$), the alkalinity should have originated elsewhere. The waters with the lowest $\delta^{13}\text{C}$ in the Last Glacial Maximum (LGM) are in the deep Atlantic Southern Ocean (Hodell et al., 2003). Sosdian et al. (2018) proposed that these corrosive waters filled the Atlantic basin during glacials, dissolving sedimentary carbonate and raising the $[\text{CO}_3^{2-}]$ and alkalinity. Glacial Atlantic overturning circulation with a shoaled flow to the Southern Ocean (Thornalley et al., 2013) may have carried these waters with high $[\text{CO}_3^{2-}]$ and increased alkalinity to the upper Pacific overturning cell by way of the Antarctic Circumpolar Current (Sosdian et al., 2018). The higher Sr/Ca- ΔCO_3 within the latter half of glacial periods may be a signal of increased $[\text{CO}_3^{2-}]$ and alkalinity from the Atlantic, rather than a ventilation signal. This pattern shows up more clearly in the ΔCO_3 derived from Sr/Ca than B/Ca. The rise in $\delta^{13}\text{C}$ over the latter half of the glacial at both sites may be the result of a change in the balance between remineralization of organic matter which reduces $\delta^{13}\text{C}$ and ventilation which increases $\delta^{13}\text{C}$.

Studies that infer respired carbon (Clementi & Sikes, 2019; Ronge et al., 2015), dissolved oxygen (Anderson et al., 2019; Jacobel et al., 2017), and water-mass ventilation age (Rafter et al., 2022; Ronge et al., 2016) suggest increased carbon storage in the interior Pacific Ocean during the LGM (Jacobel et al., 2019). Presently, the oldest waters in the Pacific basin are found at $\sim 2,000$ m depth, but during the LGM were centered at $\sim 2,500$ – $3,000$ m (Rafter et al., 2022; Ronge et al., 2016). The vertical extent of Pacific sub-surface water masses shifted between glacial and interglacial periods (Ronge et al., 2015), and based on offsets in $\delta^{13}\text{C}$ and $\delta^{18}\text{O}$, Clementi and Sikes (2019) proposed that intermediate depths (1.1–2.0 km) were denser and more isolated from the atmosphere (i.e., less ventilated) compared with the modern ocean, whereas shallower mode waters freshened and remained in communication with the atmosphere and the locus of high stratification likely shoaled during the LGM, allowing intermediate and upper deep waters to sequester more CO_2 from the atmosphere. The increased glacial offset in $\delta^{18}\text{O}$ between U1487 (874 m depth) and U1486 (1,332 m depth) is consistent with this proposal. In addition, slower glacial overturning circulation increased the water-mass age and respired carbon in these waters, which comprised the upper cell in the glacial Pacific (Allen et al., 2020; Rafter et al., 2022). In a southwest Pacific depth transect, a peak in offset $\delta^{13}\text{C}$ from upper waters and a subsequent sharp rise in offset $\delta^{13}\text{C}$ from deeper intermediate waters were both coincident with a rapid atmospheric rise in CO_2 during HS1 (Clementi & Sikes, 2019). Based on benthic foraminiferal B/Ca records from this same depth transect, Allen et al. (2020) argued for enhanced storage of respired CO_2 at water depths of ~ 1.2 – 2.5 km below the surface and showed that the major rise in atmospheric CO_2 during HS1 was associated with increases in $\delta^{13}\text{C}$ and peaks in the ΔCO_3 record. Our new Sr/Ca- ΔCO_3 records from U1486 (1,332 m), U1487 (874 m), and DSDP 593 (1,089 m) show peaks that are concurrent with the steep rise in atmospheric CO_2 around the last Termination (Figures 7a and 7b). The peak from the shallower site U1487 precedes the peaks from the deeper sites, implying CO_2 is released from shallower ocean depths first, consistent with the pattern noticed by Clementi and Sikes (2019). Notably, we extend the existing records of CO_2 storage in intermediate water back 350 ky and find that the same pattern in peak sequence also occurs during the previous two terminations. The peaks appear to precede Termination III, but the timing of that termination is not as well constrained (Raymo et al., 1997). These results suggest that intermediate depths likely play a key role in Southern Ocean and South Pacific basin carbon cycling on G-IG timescales.

7. Summary and Conclusions

Our down-core and core-top records support previous studies, suggesting that Sr/Ca ratios in the benthic foraminifera *P. wuellerstorfi* are controlled to a large degree by changes in bottom water ΔCO_3 , with no detectable influence of temperature. Despite the offsets between calibrations for various basins, we conclude that Sr/Ca may be a useful proxy for ΔCO_3 as it may offer additional paleoceanographic insights to the B/Ca record of deep ocean ΔCO_3 . As Sr^{2+} substitutes for Ca^{2+} whereas $\text{B}(\text{OH})_4^-$ substitutes for CO_3^{2-} , the pathways of these trace element ions into foraminiferal calcite and the causes for the carbonate ion sensitivity are likely different.

We demonstrate the utility of the Sr/Ca proxy through the reconstruction of the western equatorial Pacific intermediate and upper deep water ΔCO_3 records. These reveal relatively high ΔCO_3 during glacials and low ΔCO_3 during interglacials, consistent with elevated alkalinity in the glacial Southern Ocean, and consistent with a different glacial circulation pattern for the intermediate and upper deep Pacific. Coupled with benthic foraminiferal $\delta^{13}\text{C}$ records from these cores, we suggest that there was increased carbon storage in the western equatorial

Pacific during the past four glacial intervals. Spikes in Sr/Ca-derived ΔCO_3 at Terminations I, II, and III in upper deep water coincide with a rapid increase in atmospheric $p\text{CO}_2$, indicating that carbon stored in upper deep waters of the equatorial Pacific during glacial intervals contributed to the deglacial release of CO_2 from the Southern Ocean. Increasing intermediate water ΔCO_3 before these spikes suggests that CO_2 release started from upper water and progressed deeper into the Pacific Ocean interior.

We also demonstrate that the incorporation of sulfur into *P. wuellerstorfi* during calcite biomineralization is affected by both temperature and saturation state, having opposing effects, and so S/Ca would not likely yield a useful proxy for ΔCO_3 . Nonetheless, assuming that the relationships with ΔCO_3 and temperature remain the same in the past, sulfur in foraminiferal calcite presents the possibility of reconstructing a long-term (e.g., Cenozoic) record of sulfate in the ocean.

Finally, we show that biomineralization of Mg/Ca into *P. wuellerstorfi* calcite is affected by both temperature and saturation state. These effects work in opposition to mute the Mg/Ca signal from the benthic foraminiferal *P. wuellerstorfi* calcite, rendering it an inaccurate proxy for bottom water temperatures in the western equatorial Pacific.

Data Availability Statement

Upon publication, isotope and trace elemental data from this study will be made publicly available at the NOAA World Data Service for Paleoclimatology offered through the National Centers for Environmental Information (U1486 data, U1487 data, and new Sr/Ca core-top data paired with modern ΔCO_3 ; <https://www.ncei.noaa.gov/access/paleo-search/study/39727>; new DSDP 593 Sr/Ca data: <https://www.ncei.noaa.gov/access/paleo-search/study/38819>).

Acknowledgments

Research funding was provided by NSF Grant OCE-1834208 (Y. Rosenthal). Funding for research on DSDP 593 was supported by the UK Natural Environment Research Council (awards NE/I027703/1 and IP-1339-1112 to E. L. McClymont and NE/I024372/1 to S. Kender) and a Philip Leverhulme Prize (awarded to E. L. McClymont). The authors wish to thank Lois Merritt, Laura Haynes, Mervyn Graves, Sev Kender, and the late Harry Elderfield for their assistance.

References

- Allen, K. A., Hönisch, B., Eggins, S. M., & Rosenthal, Y. (2012). Environmental controls on B/Ca in calcite tests of the tropical planktic foraminifer species *Globigerinoides ruber* and *Globigerinoides sacculifer*. *Earth and Planetary Science Letters*, 351–352, 270–280. <https://doi.org/10.1016/j.epsl.2012.07.004>
- Allen, K. A., Sikes, E. L., Anderson, R. F., & Rosenthal, Y. (2020). Rapid loss of CO_2 from the South Pacific Ocean during the last glacial termination. *Paleoceanography and Paleoclimatology*, 35(2), 1–13. <https://doi.org/10.1029/2019PA003766>
- Anderson, R. F., Sachs, J. P., Fleisher, M. Q., Allen, K. A., Yu, J., Koutavas, A., & Jaccard, S. L. (2019). Deep-Sea oxygen depletion and ocean carbon sequestration during the last ice age. *Global Biogeochemical Cycles*, 33(3), 301–317. <https://doi.org/10.1029/2018GB006049>
- Babila, T. L., Rosenthal, Y., & Conte, M. H. (2014). Evaluation of the biogeochemical controls on B/Ca of globigerinoides ruber white from the oceanic flux Program, Bermuda. *Earth and Planetary Science Letters*, 404, 67–76. <https://doi.org/10.1016/j.epsl.2014.05.053>
- Bainbridge, A. E. (1981). *GEOSECS Atlantic expedition, Volume 1, hydrographic data*. National Science Foundation.
- Bereiter, B., Eggelston, S., Schmitt, J., Nehrass-Ahles, C., Stocker, T. F., Fischer, H., et al. (2015). Revision of the EPICA Dome C CO_2 record from 800 to 600-kyr before present. *Geophysical Research Letters*, 42(2), 542–549. <https://doi.org/10.1002/2014GL01957>
- Berger, W. H. (1977). Deep-sea carbonate and the deglaciation preservation spike in pteropods and foraminifera. *Nature*, 269(5626), 301–304. <https://doi.org/10.1038/269301a0>
- Berry, J. N. (1998). Sulfate in foraminiferal calcium carbonate: Investigating a potential proxy for sea water carbonate ion concentration. In *MIT/ Woodshole (issue 1992)*.
- Broecker, W. S., Spence, D. W., & Craig, H. (1982). *GEOSECS Pacific expedition Volume 3, hydrographic data*. NSF.
- Carpenter, S. J., & Lohmann, K. C. (1992). Sr/Mg ratios of modern marine calcite: Empirical indicators of ocean chemistry and precipitation rate. *Geochimica et Cosmochimica Acta*, 56(5), 1837–1849. [https://doi.org/10.1016/0016-7037\(92\)90314-9](https://doi.org/10.1016/0016-7037(92)90314-9)
- Chapman, P. (1998). The World ocean circulation experiment (WOCE). *Marine Technology Society Journal*, 32, 23–36.
- Clementi, V. J., & Sikes, E. L. (2019). Southwest Pacific vertical structure influences on oceanic carbon storage since the last glacial maximum. *Paleoceanography and Paleoclimatology*, 34(5), 734–754. <https://doi.org/10.1029/2018PA003501>
- Elderfield, H., Ferretti, P., Greaves, M., Crowhurst, S. J., McCave, I. N., Hodell, D. A., & Piotrowski, A. M. (2012). Evolution of ocean temperature and ice volume through the Mid-Pleistocene climate transition. *Science*, 337(6095), 704–709. <https://doi.org/10.1126/SCIENCE.1219444>
- Elderfield, H., Greaves, M., Barker, S., Hall, I. R., Tripati, A., Ferretti, P., et al. (2010). A record of bottom water temperature and seawater $\delta^{18}\text{O}$ for the Southern Ocean over the past 440 kyr based on Mg/Ca of benthic foraminiferal *Uvigerina* spp. *Quaternary Science Reviews*, 29(1–2), 160–169. <https://doi.org/10.1016/j.quascirev.2009.07.013>
- Elderfield, H., Yu, J., Anand, P., Kiefer, T., & Nyland, B. (2006). Calibrations for benthic foraminiferal Mg/Ca paleothermometry and the carbonate ion hypothesis. *Earth and Planetary Science Letters*, 250(3–4), 633–649. <https://doi.org/10.1016/j.epsl.2006.07.041>
- Elmore, A. C., McClymont, E. L., Elderfield, H., Kender, S., Cook, M. R., Leng, M. J., et al. (2015). Antarctic Intermediate Water properties since 400 ka recorded in infaunal (*Uvigerina peregrina*) and epifaunal (*Planulina wuellerstorfi*) benthic foraminifera. *Earth and Planetary Science Letters*, 428, 193–203. <https://doi.org/10.1016/j.epsl.2015.07.013>
- Erez, J. (2003). The source of ions for biomineralization in foraminifera and their implications for paleoceanographic proxies. *Reviews in Mineralogy and Geochemistry*, 54(1), 115–149. <https://doi.org/10.2113/0540115>
- Ford, H. L., Sosdian, S. M., Rosenthal, Y., & Raymo, M. E. (2016). Gradual and abrupt changes during the mid-Pleistocene transition. *Quaternary Science Reviews*, 148, 222–233. <https://doi.org/10.1016/j.quascirev.2016.07.005>

- Hemming, N. G., & Hanson, G. N. (1992). Boron isotopic composition and concentration in modern marine carbonates. *Geochimica et Cosmochimica Acta*, 56(1), 537–543. [https://doi.org/10.1016/0016-7037\(92\)90151-8](https://doi.org/10.1016/0016-7037(92)90151-8)
- Hodell, D. A., Venz, K. A., Charles, C. D., & Ninnemann, U. S. (2003). Pleistocene vertical carbon isotope and carbonate gradients in the South Atlantic sector of the Southern Ocean. *Geochemistry, Geophysics, Geosystems*, 4(1), 1–19. <https://doi.org/10.1029/2002GC000367>
- Jacobel, A. W., Anderson, R. F., & Jaccard, S. L. (2019). Ice-age storage of respired carbon in the Pacific Ocean. *Past Global Changes Magazine*, 27(2), 2018–2019. <https://doi.org/10.22498/pages.27.2.52>
- Jacobel, A. W., McManus, J. F., Anderson, R. F., & Winckler, G. (2017). Repeated storage of respired carbon in the equatorial Pacific Ocean over the last three glacial cycles. *Nature Communications*, 8(1), 1727. <https://doi.org/10.1038/s41467-017-01938-x>
- Keul, N., Langer, G., Thoms, S., de Nooijer, L. J., Reichart, G. J., & Bijma, J. (2017). Exploring foraminiferal Sr/Ca as a new carbonate system proxy. *Geochimica et Cosmochimica Acta*, 202, 374–386. <https://doi.org/10.1016/j.gca.2016.11.022>
- Lambert, J. E., Gibson, K. A., Linsley, B. K., Bova, S. C., Rosenthal, Y., & Surprenant, M. (2022). Equatorial Pacific bulk sediment $\delta^{15}\text{N}$ supports a secular increase in Southern Ocean nitrate utilization after the mid-Pleistocene Transition. *Quaternary Science Reviews*, 278, 107348. <https://doi.org/10.1016/j.quascirev.2021.107348>
- Lambert, J. E., Linsley, B. K., Abell, J. T., Bova, S. C., Winckler, G., Rosenthal, Y., et al. (2023). Obliquity-driven subtropical forcing of the thermocline after 240 ka in the southern sector of the Western Pacific Warm Pool. *Palaeogeography, Palaeoclimatology, Palaeoecology*, 621(April), 111578. <https://doi.org/10.1016/j.palaeo.2023.111578>
- Lear, C. H., Rosenthal, Y., & Slowey, N. (2002). Benthic foraminiferal Mg/Ca-paleothermometry: A revised core-top calibration. *Geochimica et Cosmochimica Acta*, 66(19), 3375–3387. [https://doi.org/10.1016/S0016-7037\(02\)00941-9](https://doi.org/10.1016/S0016-7037(02)00941-9)
- Lisiecki, L. E., & Raymo, M. E. (2005). A Pliocene-Pleistocene stack of 57 globally distributed benthic $\delta^{18}\text{O}$ records. *Paleoceanography*, 20(1), PA1003. <https://doi.org/10.1029/2004PA001071>
- Lo Giudice Cappelli, E., Regenber, M., Holbourn, A., Kuhnt, W., Garbe-Schönberg, D., & Andersen, N. (2015). Refining *C. wuellerstorfi* and *H. elegans* Mg/Ca temperature calibrations. *Marine Micropaleontology*, 121, 70–84. <https://doi.org/10.1016/j.marmicro.2015.10.001>
- Lüthi, D., Le Floch, M., Bereiter, B., Blunier, T., Barnola, J. M., Siegenthaler, U., et al. (2008). High-resolution carbon dioxide concentration record 650,000–800,000 years before present. *Nature*, 453(7193), 379–382. <https://doi.org/10.1038/nature06949>
- Martin, P. A., Lea, D. W., Rosenthal, Y., Shackleton, N. J., Sarnthein, M., & Papenfuss, T. (2002). Quaternary deep sea temperature histories derived from benthic foraminiferal Mg/Ca. *Earth and Planetary Science Letters*, 198(1–2), 193–209. [https://doi.org/10.1016/S0012-821X\(02\)00472-7](https://doi.org/10.1016/S0012-821X(02)00472-7)
- McClymont, E. L., Elmore, A. C., Kender, S., Leng, M. J., Greaves, M., & Elderfield, H. (2016). Pliocene-Pleistocene evolution of sea surface and intermediate water temperatures from the southwest Pacific. *Paleoceanography*, 31(6), 895–913. <https://doi.org/10.1002/2016PA002954>
- Misra, S., Greaves, M., Owen, R., Kerr, J., Elmore, A. C., & Elderfield, H. (2014). Determination of B/Ca of natural carbonates by HR-ICP-MS. *Geochemistry, Geophysics, Geosystems*, 15(4), 1617–1628. <https://doi.org/10.1002/2013GC005049>
- Naidu, P. D., Singh, A. D., Ganeshram, R., & Bharti, S. K. (2014). Abrupt climate-induced changes in carbonate burial in the Arabian Sea: Causes and consequences. *Geochemistry, Geophysics, Geosystems*, 15(4), 1398–1406. <https://doi.org/10.1002/2013GC005065>
- Nürnberg, D., Buma, J., & Hemleben, C. (1996). Assessing the reliability of magnesium in foraminiferal calcite as a proxy for water mass temperatures. *Geochimica et Cosmochimica Acta*, 60(5), 803–814. [https://doi.org/10.1016/0016-7037\(95\)00446-7](https://doi.org/10.1016/0016-7037(95)00446-7)
- Olsen, A., Lange, N., Key, R., Tanhua, T., Bittig, H., Kozyr, A., et al. (2020). GLODAPv2.2020—The second update of GLODAPv2. In *Earth system science data discussions*, July (pp. 1–41).
- Olsen, A., Lange, N., Key, R. M., Tanhua, T., Alvarez, M., Becker, S., et al. (2019). GLODAPv2.2019—an update of GLODAPv2. *Earth System Science Data*, 11, 1437–1461. <https://doi.org/10.5194/essd-2019-66>
- Petit, J. R., Raynaud, D., Basile, I., Chappellaz, J., Ritz, C., Delmotte, M., et al. (1999). Climate and atmospheric history of the past 420,000 years from the Vostok ice core, Antarctica. *Nature*, 399(6735), 429–436. <https://doi.org/10.1038/20859>
- Pingitore, N. E., Jr., Meitzner, G., & Love, K. (1995). Identification of sulfate in natural carbonates by X-ray absorption spectroscopy. *Geochimica et Cosmochimica Acta*, 59(12), 2477–2483. [https://doi.org/10.1016/0016-7037\(95\)00142-5](https://doi.org/10.1016/0016-7037(95)00142-5)
- Rae, J. W. B., Foster, G. L., Schmidt, D. N., & Elliott, T. (2011). Boron isotopes and B/Ca in benthic foraminifera: Proxies for the deep ocean carbonate system. *Earth and Planetary Science Letters*, 302(3–4), 403–413. <https://doi.org/10.1016/j.epsl.2010.12.034>
- Rafter, P. A., Gray, W. R., Hines, S. K. V., Burke, A., Costa, K. M., Gottschalk, J., et al. (2022). Global reorganization of deep-sea circulation and carbon storage after the last ice age. *Science Advances*, 8(46), 1–10. <https://doi.org/10.1126/sciadv.abq5434>
- Raymo, M. E., Oppo, D. W., & Curry, W. (1997). The mid-Pleistocene climate transition: A deep sea carbon isotopic perspective. *Paleoceanography*, 12(4), 546–559. <https://doi.org/10.1029/97pa01019>
- Rickaby, R. E. M., Elderfield, H., Roberts, N., Hillenbrand, C. D., & Mackensen, A. (2010). Evidence for elevated alkalinity in the glacial Southern Ocean. *Paleoceanography*, 25(1), 1–15. <https://doi.org/10.1029/2009PA001762>
- Ronge, T. A., Steph, S., Tiedemann, R., Prange, M., Merkel, U., Nürnberg, D., & Kuhn, G. (2015). Pushing the boundaries: Glacial/interglacial variability of intermediate and deep waters in the southwest Pacific over the last 350,000 years. *Paleoceanography*, 30(2), 23–38. <https://doi.org/10.1002/2014PA002727>
- Ronge, T. A., Tiedemann, R., Lamy, F., Köhler, P., Alloway, B. V., De Pol-Holz, R., et al. (2016). Radiocarbon constraints on the extent and evolution of the South Pacific glacial carbon pool. *Nature Communications*, 7(May), 1–12. <https://doi.org/10.1038/ncomms11487>
- Rosenthal, Y., Boyle, E. A., & Slowey, N. (1997). Temperature control on the incorporation of magnesium, strontium, fluorine, and cadmium into benthic foraminiferal shells from Little Bahama Bank: Prospects for thermocline paleoceanography. *Geochimica et Cosmochimica Acta*, 61(17), 3633–3643. [https://doi.org/10.1016/s0016-7037\(97\)00181-6](https://doi.org/10.1016/s0016-7037(97)00181-6)
- Rosenthal, Y., Field, M. P., & Sherrell, R. M. (1999). Precise determination of element/calcium ratios in calcareous samples using sector field inductively coupled plasma mass spectrometry. *Analytical Chemistry*, 71(15), 3248–3253. <https://doi.org/10.1021/ac981410x>
- Rosenthal, Y., Holbourn, A., Kulhanek, D. K., & Scientists, E. (2018). *Proceedings of the international ocean discovery program* (Vol. 363). Western Pacific Warm Pool. <https://doi.org/10.14379/iodp.proc.363.2018>
- Rosenthal, Y., Lear, C. H., Oppo, D. W., & Linsley, B. K. (2006). Temperature and carbonate ion effects on Mg/Ca and Sr/Ca ratios in benthic foraminifera: Aragonitic species *Hoeglundina elegans*. *Paleoceanography*, 21(1), 1–14. <https://doi.org/10.1029/2005PA001158>
- Rosenthal, Y., Perron-Cashman, S., Lear, C. H., Bard, E., Barker, S., Billups, K., et al. (2004). Interlaboratory comparison study of Mg/Ca and Sr/Ca measurements in planktonic foraminifera for paleoceanographic research. *Geochemistry, Geophysics, Geosystems*, 5(4), 1–29. <https://doi.org/10.1029/2003GC000650>
- Ryan, W. B. F., Carbotte, S. M., Coplan, J., O'Hara, S., Melkonian, A., Arko, R., et al. (2009). Global Multi-Resolution Topography (GMRT) synthesis data set. *Geochemistry, Geophysics, Geosystems*, 10(3), Q03014. <https://doi.org/10.1029/2008GC002332>
- Schlitzer, R. (2018). Ocean data View. Retrieved from <https://odv.awi.de>

- Sharp, J. D., Pierrot, D., Humphreys, M. P., Epitalon, J.-M., Orr, J. C., Lewis, E., & Wallace, D. W. R. (2020). *CO2SYS.v3 (No. CO₂-system-ExtD, v3.0)*. MathWorks.
- Siegenthaler, U., Stocker, T. F., Monnin, E., Luthi, D., Schwander, J., Stauffer, B., et al. (2005). Stable carbon cycle—Climate relationship during the late Pleistocene. *Science*, *310*(November), 1313–1317. <https://doi.org/10.1126/science.1120130>
- Sosdian, S., & Rosenthal, Y. (2010). Response to comment on “deep-sea temperature and ice volume changes across the Pliocene-Pleistocene climate transitions”. *Science*, *328*(June), 1480. <https://doi.org/10.1126/science.1186768>
- Sosdian, S. M., & Rosenthal, Y. (2009). Deep-Sea temperature and ice volume changes across the Pliocene-Pleistocene climate transitions. *Science*, *325*(5938), 306–310. <https://doi.org/10.1126/science.1169938>
- Sosdian, S. M., Rosenthal, Y., & Toggweiler, J. R. (2018). Deep Atlantic carbonate ion and CaCO₃ compensation during the ice ages. *Paleoceanography and Paleoclimatology*, *33*(6), 546–562. <https://doi.org/10.1029/2017PA003312>
- Stirpe, C. R., Allen, K. A., Sikes, E. L., Zhou, X., Rosenthal, Y., Cruz-Uribe, A. M., & Brooks, H. L. (2021). The Mg/Ca proxy for temperature: A Uvigerina core-top study in the southwest Pacific. *Geochimica et Cosmochimica Acta*, *309*, 299–312. <https://doi.org/10.1016/j.gca.2021.06.015>
- Tachikawa, K., Cartapanis, O., Vidal, L., Beaufort, L., Barlyaeva, T., & Bard, E. (2011). The precession phase of hydrological variability in the Western Pacific Warm Pool during the past 400 ka. *Quaternary Science Reviews*, *30*(25–26), 3716–3727. <https://doi.org/10.1016/j.quascirev.2011.09.016>
- Thornalley, D. J. R., Barker, S., Becker, J., Hall, I. R., & Knorr, G. (2013). Abrupt changes in deep Atlantic circulation during the transition to full glacial conditions. *Paleoceanography*, *28*(2), 253–262. <https://doi.org/10.1002/palo.20025>
- Tsuchiya, M. (1991). Flow path of the Antarctic intermediate water in the western equatorial South Pacific Ocean. *Deep-Sea Research, Part A: Oceanographic Research Papers*, *38*(1965), S273–S279. [https://doi.org/10.1016/s0198-0149\(12\)80013-6](https://doi.org/10.1016/s0198-0149(12)80013-6)
- Uchikawa, J., Penman, D. E., Zachos, J. C., & Zeebe, R. E. (2015). Experimental evidence for kinetic effects on B/Ca in synthetic calcite: Implications for potential B(OH)⁴⁻ and B(OH)³ incorporation. *Geochimica et Cosmochimica Acta*, *150*, 171–191. <https://doi.org/10.1016/j.gca.2014.11.022>
- van Dijk, I., de Nooijer, L. J., Boer, W., & Reichert, G. J. (2017). Sulfur in foraminiferal calcite as a potential proxy for seawater carbonate ion concentration. *Earth and Planetary Science Letters*, *470*, 64–72. <https://doi.org/10.1016/j.epsl.2017.04.031>
- Weiss, R. F., Broecker, W. S., Craig, H., & Spencer, D. W. (1983). *GEOSECS Indian Ocean Expedition Volume 5, hydrographic data*. NSF.
- Wollenburg, J. E., Raitzsch, M., & Tiedemann, R. (2015). Novel high-pressure culture experiments on deep-sea benthic foraminifera—Evidence for methane seepage-related δ¹³C of Cibicides wuellerstorfi. *Marine Micropaleontology*, *117*, 47–64. <https://doi.org/10.1016/j.marmicro.2015.04.003>
- Wyrki, K. (1961). The subsurface water masses in the western South Pacific Ocean. *Marine and Freshwater Research*, *13*(1), 18–47. <https://doi.org/10.1071/MF9620018>
- Yu, J., Anderson, R. F., & Rohling, E. J. (2014). Deep Ocean carbonate chemistry and glacial-interglacial atmospheric CO₂ changes. *Oceanography*, *27*(1), 16–25. <https://doi.org/10.5670/oceanog.2014.04>
- Yu, J., Broecker, W. S., Elderfield, H., Jin, Z., McManus, J., & Zhang, F. (2010). Loss of carbon from the deep sea since the last glacial maximum. *Science*, *330*(6007), 1084–1087. <https://doi.org/10.1126/science.1193221>
- Yu, J., & Elderfield, H. (2007). Benthic foraminiferal B/Ca ratios reflect deep water carbonate saturation state. *Earth and Planetary Science Letters*, *258*(1–2), 73–86. <https://doi.org/10.1016/j.epsl.2007.03.025>
- Yu, J., & Elderfield, H. (2008). Mg/Ca in the benthic foraminifera *Cibicidoides wuellerstorfi* and *Cibicidoides mundulus*: Temperature versus carbonate ion saturation. *Earth and Planetary Science Letters*, *276*(1–2), 129–139. <https://doi.org/10.1016/j.epsl.2008.09.015>
- Yu, J., Elderfield, H., Jin, Z., Tomascak, P., & Rohling, E. J. (2014). Controls on Sr/Ca in benthic foraminifera and implications for seawater Sr/Ca during the late Pleistocene. *Quaternary Science Reviews*, *98*, 1–6. <https://doi.org/10.1016/j.quascirev.2014.05.018>